Dynamics of multimode semiconductor lasers

A. M. Yacomotti, L. Furfaro, X. Hachair, F. Pedaci, M. Giudici, J. Tredicce, J. Javaloyes, and S. Balle*
Institut Non-linéaire de Nice, UMR 6618 Centre National de la Recherche Scientifique, Université de Nice Sophia-Antipolis, 06560 Valbonne, France

E. A. Viktorov and Paul Mandel
Optique nonlinéaire théorique, Université Libre de Bruxelles, Campus Plaine Code Postale 231, B-1050 Bruxelles, Belgium
(Received 14 June 2002; revised manuscript received 26 August 2003; published 24 May 2004)

We analyze multi-longitudinal-mode semiconductor lasers experimentally. We show that the intensity of each mode displays large amplitude oscillations but obeys a highly organized antiphase dynamics leading to an almost constant total intensity output. For each mode, regular switching is observed in the megahertz range, while the optical frequency as a function of time follows a well defined sequence from blue to red. Using a multimode theoretical model, we identify that four-wave mixing is the dominant mechanism at the origin of the observed dynamics. The asymmetry of the susceptibility function of semiconductor materials allows us to explain the optical frequency sequence.

DOI: 10.1103/PhysRevA.69.053816 PACS number(s): 42.60.Mi, 05.45.−a

I. INTRODUCTION

The performance of optical systems using semiconductor lasers for communications or measurements is limited by power fluctuations. At a fundamental level, the two main sources of power fluctuations have been assigned to mode partition and mode hopping for multimode lasers. Mode partition explains anticorrelated fluctuations between the main mode and weak side modes [1,2]. Its result is the enhancement of the individual mode intensity noise, while the noise of the total output remains relatively small. It has also been demonstrated that mode partition noise limits information transmission at any rate [3]. Recently, it was shown that mode partition can be spectrally asymmetric [4] and can even affect quantum noise partition [5]. Mode hopping has been observed and described as sudden drop-offs of the main mode output power, associated with the excitation of a side mode. It results in irregular switching between the main mode and a side mode, although the total intensity remains nearly constant [6]. Since it is detrimental for applications that semiconductor lasers naturally emit in several longitudinal modes, the problem of multimode operation has been actively discussed, and both mode partition and mode hopping have been successfully interpreted via stochastic theories as noise-induced phenomena originating from spontaneous emission and mode coupling [7–10].

In this paper we report, for the first time to our knowledge, on the existence of deterministic nonlinear dynamics in a free-running multimode semiconductor laser. The main dynamical effects found in a set of experiments realized with different lasers are (i) there are periodic intensity fluctuations, in the megahertz range, of each modal output; (ii) there is compensation in the total output, which remains practically constant in time; (iii) the switching sequence follows the modal optical frequencies from blue to red; when the reddest mode switches off, the sequence restarts from the bluest mode. These effects are robust against a change of the control parameters which mostly affects the number of oscillating modes. For example, on increasing the pump current, the property of regular mode switching is maintained and the total intensity remains constant independently of the numbers of oscillating modes up to seven. For larger numbers of oscillating modes, the fluctuations persist, but they can lose regularity in phase and amplitude.

These experimental results cannot be explained in the frame of the stochastic theory that was previously used for mode-hopping or mode-partition studies. In order to explain the observations, we consider a multimode model that includes the optical susceptibility of quantum-well semiconductor media [11] and four-wave-mixing processes among the laser modes. A simpler phenomenological model allows clear identification of the dominant mechanisms. The numerical results obtained with both models qualitatively reproduce all the experimentally observed features.

II. EXPERIMENTAL RESULTS

The experimental setup is shown in Fig. 1. We tested several 850 nm, quantum-well, edge-emitting lasers of two models: Roithner™ RTL8510MG and SDL™ 5400C. The separation between two consecutive longitudinal modes is 130 GHz for the first laser type and 60 GHz for the second. The laser package temperature was stabilized to 0.01 °C and the laser current was controlled with a very stable (to 0.001 mA) power supply. The lasers operate on a variable number of longitudinal modes, depending on the pumping current and on temperature. We have explored injection currents $I_{th} < I < 1.8 I_{th}$ and temperatures from 15 °C to 25 °C: in this range of control parameters the number of active modes varies from one to seven. The total intensity output of the lasers is monitored with an avalanche photodiode

*On sabbatical leave from Institut Mediterrani d'Estudis Avançats, IMEDEA (CSIC-UIB), C/Miquel Marqués 21, E-07190 Esporles, Spain.

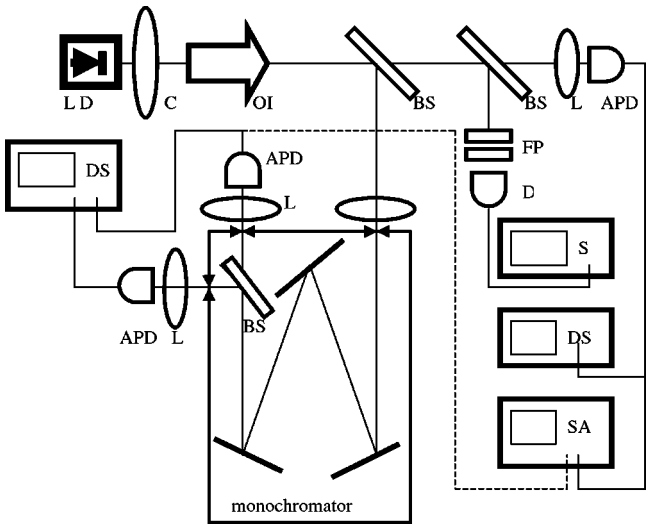

FIG. 1. Experimental setup: LD, laser diode; C, collimator; OI, optical isolator; BS, beam splitter; L, lens; APD, avalanche photodiode 2 GHz; FP, Fabry-Pérot interferometer; D, detector; S, oscilloscope; DS, digital oscilloscope; SA, spectrum analyzer.

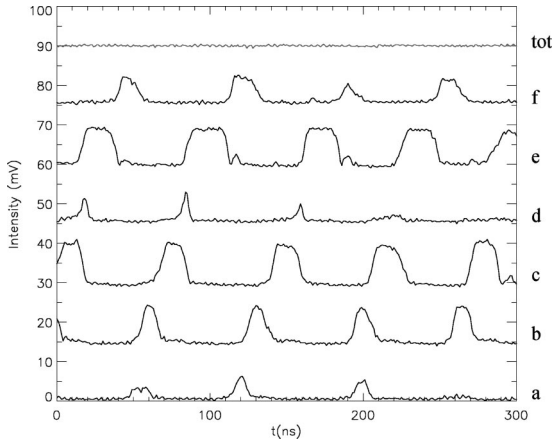

FIG. 2. Modal intensity behavior. The modes $a-f$ detected are shown from the bluest to the reddest (from bottom to top) and can be related to the labels in the optical spectrum of Fig. 3. At the top we plot the total intensity output (gray line). We have displaced vertically the intensity traces of modes $b-f$ by opportune offset (15 mV for *b*, 30 mV for *c*, and so on, by multiples of 15 mV) to avoid overlapping the five traces. The total intensity has been displaced by an offset of 80 mV. The laser pump is about 60% over the threshold and the temperature is 19 °C.

(2 GHz bandwidth), and a scanning Fabry-Pérot interferometer is used to determine the number of oscillating modes. Part of the beam is sent to a monochromator having two separate output slits. Each slit can be moved in order to select a central frequency. The width of the slits has been set to filter a frequency band of 30 GHz around the selected central frequency. This setting allows for filtering a single longitudinal mode at the slit output for both types of lasers tested. A fast avalanche photodiode detector (2 GHz bandwidth) is placed behind each slit. After proper positioning of the slits, real-time monitoring of two different longitudinal modal intensities is possible. The two timeseries are recorded on a LeCroy Wavepro digital scope (2 GHz analog bandwidth, 8 GHz digital bandwidth). The power spectra of the signals are monitored using an Agilent E4403B spectrum analyzer. Since there is no delay between the two optoelectronic paths of modal detection, we can directly compare the dynamics of each mode with the one recorded in the same acquisition.

When the modal dynamics is regular, we are able to reconstruct the real-time dynamics of all the modes in a significant time window. We fix the first slit in order to filter one of the main active longitudinal modes, while the second slit is repositioned at each acquisition in order to filter a different longitudinal mode. In this way the time series of each active mode is acquired together with the corresponding time series of the mode filtered by the first slit. Since this mode is always present in all the acquisitions we call it the reference mode. We build an algorithm that identifies time segments of the reference mode that are recurrent in all the acquisitions. Due to the high degree of correlation between the modes, time segments of different modes (and therefore obtained in different acquisitions) may be compared provided that the corresponding time segments of the reference mode are identical in all the acquisitions. The reliability of this method of comparison is assessed by the duration of the recurrent time segments identified, which is a consequence of the regularity of modal dynamics. We have retained only those time segments whose duration is at least 300 ns, corresponding approximately to four periods of the modal switching sequence. In this time window we are able to reconstruct the real-time dynamics of all the active modes. The intensity of each mode and the total intensity output as a function of time are shown in Fig. 2. Figure 3 (left panel) shows the corresponding optical spectrum of the laser: each active mode is labeled in order to trace its dynamics in Fig. 2. In the right panel of Fig. 3 we plot the power spectra of the reference mode and of the total intensity: the extinction in the total intensity of the frequency peak relative to the modal switching is larger than −40 dB. No significant difference between the power spectra of the different modal amplitudes was observed.

The results of Figs. 2 and 3 are qualitatively the same for different parameters and for different numbers of modes. We always noticed the almost complete extinction (larger than −40 dB) of the modal switching frequency in the total intensity and a switching sequence that progresses from the blue side of the optical spectrum to the red side. The frequency of the modal switching tends to increase with pumping current and with the number of active modes but it remains in the range 5–15 MHz. On changing parameters, the regularity of the sequence can decrease as a consequence of an increasing statistical dispersion of the switching pulse amplitude.

Figure 4 shows a simple situation with only two dominating modes. This situation is useful because the real-time dynamics can be shown without any reconstruction. Again we can remark the clean antiphase switching, its regularity, and the extinction of the switching frequency peak in the total output intensity. Figures 2–4 were obtained using the laser type Roithner RTL8510MG. Similar dynamics was observed using the laser SDL 5400C.

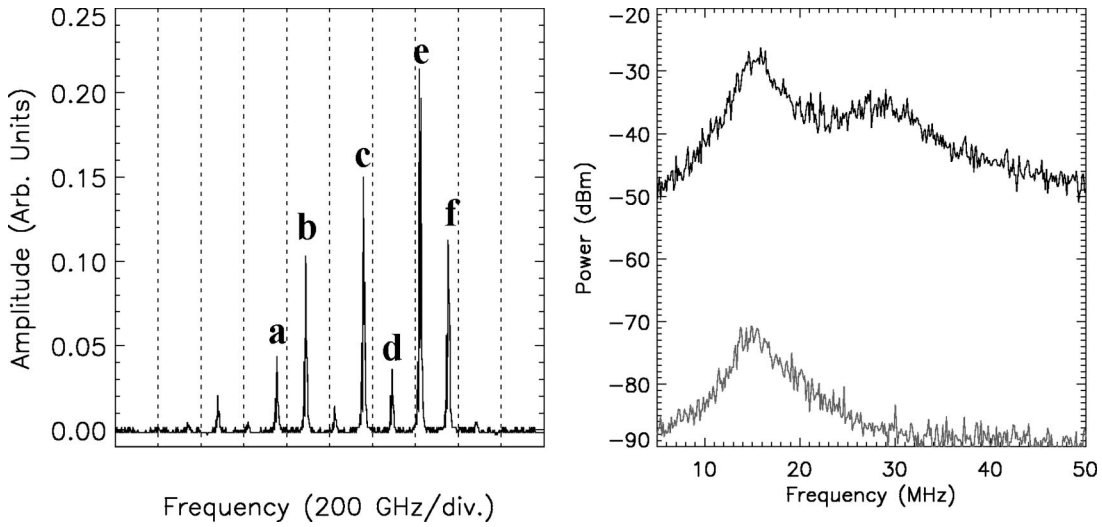

FIG. 3. Left: Optical spectrum of the laser emission relative to Fig. 2. Frequency increases from right to left. Right: Power spectra of the total intensity output (gray line) and of the modal intensity labeled *c* in Fig. 2. We used a microwave amplifier of 20 dB at the input of the spectrum analyzer.

III. BASIC EQUATIONS

Theoretical analysis of multimode operation in lasers have shown that antiphase dynamics might arise from the standing-wave interference pattern of the forward and backward fields which creates a periodic distribution of the gain in the active medium [12,13]. Based on those previous results, we construct a model appropriate for semiconductor lasers. We start from the traveling-wave equations for the slowly varying amplitudes of the forward and backward optical fields $E_{\pm}$ and the Bloch equation for the carrier density N, which read

$$\partial_t E_{\pm}(z,t) \pm v_g \partial_z E_{\pm}(z,t) = \Gamma P_{\pm}(z,t) - \kappa_i E_{\pm}, \tag{1}$$

$$\partial_t N(z,t) = J - \gamma_{\|} N(z,t) - \frac{1}{2}(E_+^* P_+ + E_-^* P_- + \text{c.c.}) + D\partial_z^2 N, \tag{2}$$

where v_g is the group velocity in the waveguide, Γ is the optical confinement factor to the active region, κ_i are the internal losses, $J=I/(eV_a)$ is the density of carriers injected into the active region per unit time due to the pumping current, $\gamma_{\|}$ is the rate of spontaneous recombination of carriers, and D is the ambipolar diffusion coefficient. The boundary conditions for these equations read

$$E_+(0,t) = r_1 E_-(0,t), \tag{3}$$

$$E_-(L,t) = r_2 e^{2ik_p L} E_+(L,t), \tag{4}$$

$$\partial_z N = 0 \text{ for } z = 0, L, \tag{5}$$

where L is the total cavity length, $r_{1,2}$ are the amplitude reflection coefficients from the front and rear facets (measured from the inside to the outside), and k_p is the optical carrier wave vector, defined as $k_p=\omega_p/cn$, where ω_p is the optical carrier frequency and n is the effective index of the waveguide.

The above equations are coupled by the nonlinear polarization of the active medium induced by each of the waves, $P_{\pm}$, which is connected to the fields and carrier density by the optical susceptibility of the active medium,

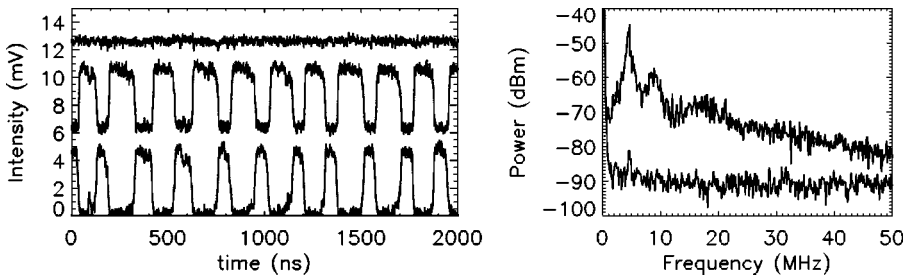

FIG. 4. Left: Modal behavior in case of two active modes, and total intensity output (top trace). The laser pump is about 50% over the threshold and the temperature is 22.4 °C. The second modal intensity trace is displaced vertically with an offset of 6 mV and the total intensity trace is displaced with an offset of 8 mV. Right: Power spectrum of the total intensity (lower trace) and of one of the two active modes (we have removed the 20 dB amplifier present in the case of Fig. 3).

$$P_{\pm}(z,t) = \frac{v_g \omega_p}{2cn} \chi\left(\omega_p + i \frac{\partial_t E_{\pm}(z,t)}{E_{\pm}(z,t)}, N(z,t) \right) E_{\pm}(z,t), \quad (6)$$

which is determined at the instantaneous frequency of the fields.

A first useful rescaling is

$$E \to \sqrt{\gamma_{\parallel}} E', \quad (7)$$

$$J \to \gamma_{\parallel} N_{eq}, \quad (8)$$

$$\chi_0 \to \left(\frac{v_g \omega_p}{2cn} \right)^{-1} \chi_0', \quad (9)$$

which gives

$$\partial_t E_{\pm}(z,t) \pm v_g \partial_z E_{\pm}(z,t) = \Gamma P_{\pm}(z,t) - \kappa_i E_{\pm}(z,t), \quad (10)$$

$$\gamma_{\parallel}^{-1} \partial_t N(z,t) = N_{eq} - N(z,t) - \frac{1}{2}(E_+^* P_+ + E_-^* P_- + \text{c.c.}) + \frac{D}{\gamma_{\parallel}} \partial_z^2 N. \quad (11)$$

We then expand the fields on the pseudo-orthogonal base of the cavity modes,

$$E_+(z,t) = \sum_j A_j(t) e^{i(q_j z - \omega_j t)}, \quad (12)$$

$$E_-(z,t) = \frac{1}{r_1} \sum_j A_j(t) e^{-i(q_j z + \omega_j t)}, \quad (13)$$

where the wave vectors q_j are determined by the boundary conditions

$$q_j = j \frac{\pi}{L} + i \kappa_{end}, \quad (14)$$

$$\kappa_{end} = \frac{1}{2L} \ln(r_1 r_2). \quad (15)$$

In the limit of the perfect cavity, q_j are real and then the basis is orthogonal. We will for simplicity assume modal orthogonality, although in this case the coupling among the modes is reduced due to neglect of the overlap of their spatial profiles [14,15].

For the modal frequencies we take

$$\omega_j = v_g q_j,$$

i.e., those determined by the dispersion relation of the cold cavity. We note that

$$\Delta\omega = v_g \frac{\pi}{L}, \quad (16)$$

$$\Delta q = \frac{\pi}{L}, \quad (17)$$

which describe the mode spacing in the device.

These equations form a base for development of multimode models in the following sections. We discuss two possible approaches leading to similar numerical results in our range of interest. The key element of both is the appearance of four-wave-mixing terms resulting from the intermode beating.

IV. PHENOMENOLOGICAL MODEL

Construction of a deterministic model has to take into account all the experimental observations reported here while remaining consistent with previous descriptions of mode partition and mode hopping. The main problem is to identify the relevant terms describing the mode coupling and the carrier population dynamics. The constant total intensity output indicates that modal anticorrelations are nearly perfect and therefore it suggests that the medium is homogeneously broadened and uniformly interacting with the field. This assumption is reinforced by the fact that material diffusion is strong in semiconductors and should wash out the effect of spatial hole burning induced by the boundary conditions of a Fabry-Pérot cavity. However, the observation of regular antiphase pulsations in the modal outputs is in conflict with this assumption because it requires a population spatial grating. Therefore we use here rate equations that couple the modal fields $A_m(t)$ to the nonlinear modal free-carrier averages $F_m(t)$. Such coupling can be interpreted as a remaining of the grating in the carrier density created by the standing waves of the field [16]. We constrain the cross-coupling parameter β_{nm} to be very close to unity to reflect the strong diffusion. Furthermore, we assume identical modal gains and losses because the gain bandwidth is between one and two orders of magnitude larger than the frequency separation among the modes. This is sufficient to induce antiphase dynamics, which has been shown to occur if a certain degree of modal degeneracy is reached [13].

We are aware of the strong simplifications we are making at this stage, but it is worthwhile to notice that this phenomenological model has the objective of identifying the necessary terms to describe the observed dynamics, remaining compatible with already known results. The same problem arises for almost all models of multimode lasers. Rate equation models have proved most useful for lasers. One of them is the (A_m, F_m) model involving $2N$ equations if N cavity modes are lasing. It is the model used in this section. It has been the support for practically all the research on intracavity second harmonic generation [13,17–19]. For completeness, let us mention that a result based on the numerical integration of the partial differential equations will give little information about the physical mechanism generating the type of instabilities observed experimentally [20].

It is also known that spectral hole burning and carrier heating contribute to the reduction of the gain for each mode. We model it as an additional weak contribution to the saturation in the modal field equations [21].

The resulting model, however, is perfectly symmetric under the permutation of any pair of modes. Thus, if modes can switch according to one time sequence, the model built so far predicts that all modal permutations of that sequence are

equally probable switching sequences [13]. Numerical integration confirmed that there is no spontaneous symmetry breaking leading to a frequency switching from the blue to the red side of the optical spectrum. To account for the observed symmetry breaking a third nonlinearity is included in the model. It is the four-wave mixing resulting from the expansion of the nonlinear gain in terms of population pulsation [22,23].

The free-carrier $N(z,t)$ can be written as

$$N(z,t) = N_0(z,t) + \sum_n^N [N_n(z,t)\exp(in\Delta\omega t) + \text{c.c.}], \quad (18)$$

where $\Delta\omega$ is the modal separation. Adiabatic elimination of $N_n(z,t)$ gives

$$N_n(z,t) = \frac{N_0}{n\Delta\omega\gamma_\parallel^{-1}} \sum_p^{n-1} (\mathcal{L}_n + \mathcal{L}_{n+p}^*)\psi_n\psi_{n+p}A_pA_{p+n}^* \quad (19)$$

and an equation for $N_0(z,t)$ that reads

$$\gamma_\parallel^{-1}\frac{dN_0}{dt} = J - N_0 - N_0\sum_n^N \psi_n^2|A_n|^2\,\mathrm{Re}(\mathcal{L}_n), \quad (20)$$

where ψ_n is a cavity eigenfunction and $1/\mathcal{L}_m = 1 - i(\omega_m - \omega_0)/\gamma_\perp$. In first approximation $\mathcal{L}_m = 1$, which is used in this section.

The modal material polarization can be written as $P_m(t) = P_m^{(1)}(t) + P_m^{(3)}(t)$, where $P_m^{(1)}$ and $P_m^{(3)}$ are the first and the third order contributions. The first order $P_m^{(1)}(t)$ is given by [23]

$$P_m^{(1)}(t) = i\int \chi(N_0(t))A_m\psi_m^2 d\zeta = i\chi_m(N_0(t))A_m, \quad (21)$$

where $\chi(N_0(t)) = \chi'(N_0(t)) + i\chi''(N_0(t))$ is the first order contribution to the optical susceptibility of the active medium and $\chi_m(N_0(t)) = \int\chi(N_0(t))\psi_m^2 d\zeta$.

Using Eq. (19), the third order modal material polarization $P_m^{(3)}(t)$ gives the four-wave-mixing terms:

$$P_m^{(3)}(t) = \sum_{k,p} \frac{\gamma_\parallel A_kA_pA_{k+p-m}^*}{i(p-m)\Delta\omega}\int \chi^{(3)}(N_0(t))\psi_m\psi_k\psi_p\psi_{k+p-m}d\zeta, \quad (22)$$

where

$$\chi^{(3)}(N_0(t)) = \chi''(N_0(t))\partial_N\chi(N_0(t)) = \chi''(N_0(t))(-1+i\alpha)\partial_N\chi''(N_0(t))$$

is the third order contribution to the optical susceptibility and $\alpha = \partial_N\chi'(N_0(t))/\partial_N\chi''(N_0(t))$ is the linewidth enhancement factor.

After normalization, the equations describing the modal fields have the structure:

$$2\frac{dA_m}{dt} = (i\chi_m - 1)A_m + \sum_{k,p}\theta_{pm}n_{kpm}A_kA_pA_{k+p-m}^*. \quad (23)$$

The coefficient in front of the four-wave-mixing term introduces the required asymmetry. Not least important is that four-wave mixing does not affect the total output, since it induces energy redistribution among the modes of the field.

We also introduce the modal free-carrier averages $F_m(t) \sim \mathrm{Re}[\int N_0(t)\psi_m^2 d\zeta]$. Note that $F_m(t)$ are spatial harmonics, different from the temporal harmonics $N_m(t)$. The equations describing the modal carrier averages are given by

$$\eta\frac{dF_m}{dt} = J - F_m\left(1 + \sum_k^N \beta_{mk}|A_k|^2\right), \quad (24)$$

where J is the pump normalized to its threshold value, $\eta = \kappa/\gamma_\parallel$. Spatial grating is accounted for by the cross-coupling coefficients $0 \leqslant \beta_{ij} \leqslant 1$. The mode indices k, m, and p vary from 1 to N, the number of oscillating modes, operating at optical frequencies ω_m.

Let us now discuss the parameters in Eqs. (23) and (24). The restriction on the double sum in Eq. (23) is $1 \leqslant k+p-m \leqslant N$. As already explained [21], to account for spectral hole burning and carrier heating, the modal gains $F_m = \mathrm{Re}(i\chi_m)$ in the field equations have been replaced by $F_m \Rightarrow g_mF_m(1 - \epsilon\Sigma_n^N\tilde{\beta}_{mn}|A_n|^2)$ where g_m is the semiconductor linear gain profile, $\tilde{\beta}_{mm} = \beta_{mm} = 1$, and $\tilde{\beta}_{mn} = (4/3)\beta_{mn}$. The factor $4/3$ for the normalized cross-coupling constant $\tilde{\beta}_{mn}$ suggests a strong mode coupling. It has been defined and successfully used for the description of mode hopping [6,24]. This effect is not included in the modal gain equations because we verified numerically that this addition does not lead to any qualitative modification of the results due to the long carrier lifetime $\eta \gg 1$.

The mode coupling coefficients are

$$\theta_{pm}n_{kpm} = \frac{\gamma_\parallel}{i(p-m)\Delta\omega}\int\chi^{(3)}(N_0(t))\psi_m\psi_k\psi_p\psi_{k+p-m}d\zeta \simeq \frac{i(1-i\alpha)\gamma_\parallel}{(p-m)\Delta\omega}\int\chi''(N_0(t))\partial_N\chi''(N_0(t)) \times\psi_m\psi_k\psi_p\psi_{k+p-m}d\zeta,$$

with

$$\theta_{pm} = \frac{i(1-i\alpha)\gamma_\parallel}{(p-m)\Delta\omega} = \frac{i\sigma}{(p-m)\eta}(1-i\alpha),$$

where $\sigma = \kappa/\Delta\omega$. We neglect the spatial dependencies in the four-wave-mixing terms. This means that the spatial factor $n_{kpm} = \int\chi''(N_0(t))\partial_N\chi''(N_0(t))\psi_m\psi_k\psi_p\psi_{k+p-m}d\zeta$ has been approximated by 1. The validity of that simplification has been checked numerically. The α factor has been introduced in the traditional way: neither modal nor intensity dependence is included. Although, in the literature, the introduction of the α factor in the linear gain has been known to lead to two different sets of equations [10], this difference does not play any significant role in our model, and the α factor in the linear gain could even be neglected. Instead, the coefficient in front of the four-wave-mixing term accounts for symmetry breaking leading to a modal switching sequence from the blue to the red side of the optical spectrum. It is worth noting

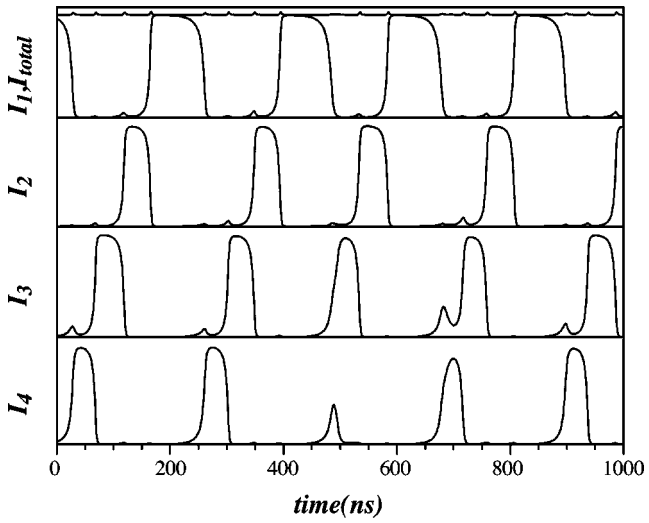

FIG. 5. Numerical results for four modes, and total intensity output. I_1 corresponds to the reddest mode. To help comparison with the experimental data, a cavity round trip time $\tau_p = 10$ ps has been assumed to fix the physical time scale.

that a negative sign of the α factor, as happens in the case of quantum dot lasers, will reverse the modal switching sequence from the red to the blue wavelength.

We have also assumed $g_m = 1$ so that the number of oscillating modes is not determined by gain or loss considerations but set arbitrarily. We have verified numerically that using weakly peaked gain profiles determines the number of modes, but does not affect the dynamical response of the laser.

The parameters used for the numerical simulations of Eqs. (23) and (24)with four modes shown in Fig. 5 are chosen to match the experimental results: $J = 1.5$, $\alpha = 2$, $\eta = 1000$, $\beta = 0.975$, $\sigma = 0.35$. The gain saturation coefficient $\epsilon = 0.05$ is derived from [7]. The oscillations have 100% modulation amplitude. They are timed regularly, and only one switching sequence from the bluest mode to the reddest mode is observed. The asymmetry of the model results in asymmetric pulsations. This effect is provided by the modulation of the carrier density at the beat optical frequency induced by the four-wave mixing in Eqs. (23) and (24). This agrees with the analysis in [25] where it was shown that four-wave mixing induces an enhancement of the gain for longer wavelengths.

V. THEORETICAL MODEL

In this section we obtain a model based on the basic equations presented in Sec. III. We project the polarization over the modes of the perfect cavity, i.e.,

$$P_+(z,t) = \sum_j B_j(t) e^{i(q_j z - \omega_j t)}. \tag{25}$$

For this purpose, we assume that—due to the large mode spacing as compared to the carrier lifetime—only the lowest beat note of the modes will be of importance in the dynamics of the carrier density, so that we consider

$$N(z,t) = N_0(t) + N_1(t) e^{i(\Delta q z - \Delta\omega t)} + N_1^*(t) e^{i(\Delta\omega t - \Delta q z)}. \tag{26}$$

In fact, the amplitude of the nth beat note is of the order of $[1 + (n\Delta\omega/\gamma_\parallel)^2]^{-1/2}$; hence we consider only the terms with $n = 0$ and $n = 1$ because for typical semiconductor laser diodes $\Delta\omega/\gamma_\parallel \gg 1$, since $\gamma_\parallel \sim 10^9\ \mathrm{s}^{-1}$, while the longitudinal mode spacing $\Delta\omega$ is of the order of 100 GHz. This approximation is equivalent to that in [26], since only the slow spatial grating in the carrier density (as represented by N_1) is dynamically included; the fast spatial grating (at half the optical wavelength) is neglected since it is strongly washed out by diffusion.

At this point, we perform a Taylor expansion of the susceptibility in both the Ω and N variables around the optical carrier frequency ω_p and N_0, respectively; hence we have

$$P_+(z,t) = \chi\left(\omega_p + i\frac{\partial_t E_+(z,t)}{E_+(z,t)}, N(z,t)\right) E_+(z,t), \tag{27}$$

$$\simeq \chi(\omega_p, N(z,t)) E_+(z,t) + i\partial_\Omega \chi(\omega_p, N(z,t)) \partial_t E_+(z,t), \tag{28}$$

$$\simeq [U + (N_1 e^{i\Phi} + N_1^* e^{-i\Phi}) V] E_+ + [U' + (N_1 e^{i\Phi} + N_1^* e^{-i\Phi}) V'] i\partial_t E_+, \tag{29}$$

where $U \equiv \chi(\omega_p, N_0(t))$, $V \equiv \partial_N \chi(\omega_p, N_0(t))$, $U' \equiv \partial_\Omega \chi(\omega_p, N_0(t))$, $V' \equiv \partial_\Omega \partial_N \chi(\omega_p, N_0(t))$, and $\Phi \equiv \Delta q z - \Delta\omega t$, and analogously we obtain the equation for P_-.

Inserting in Eq. (26) the expansion of the field in cavity modes (12) and, after summation of the different terms, we obtain

$$B_j = \chi_j A_j + \hat{\chi}_{j-1} A_{j-1} N_1 + \hat{\chi}_{j+1} A_{j+1} N_1^*, \tag{30}$$

with

$$\chi_j \equiv \chi\left(\omega_p + \omega_j + i\frac{d_t A_j}{A_j}, N_0\right) \simeq \chi(\omega_p + \omega_j, N_0), \tag{31}$$

$$\hat{\chi}_j \equiv \partial_N \chi_j, \tag{32}$$

where we have considered that the modal amplitudes change slowly as compared to the modal frequency, so that the susceptibility corresponding to each mode can be computed at the cavity frequency ω_j. As can be seen from Eq. (30), the inclusion of the spatiotemporal beat notes in the carrier density [i.e., the inclusion of the slow population grating of Eq. (26)] leads to the appearance of four-wave-mixing terms, since the polarization at the frequency of mode j now involves a contribution of the modes $j \pm 1$. Therefore, in this approach, the spatial grating term appears together with the four-wave-mixing term and the two effects cannot be separated.

Inserting Eqs. (12), (13), and (22), into Eq. (2), we obtain the dynamical equations for N_0 and N_1,

$$\gamma_\parallel^{-1} \partial_t N_0 = N_{eq} - N_0 - \sum_j (A_j^* B_j + \text{c.c.}), \tag{33}$$

$$\gamma_{\parallel}^{-1}\partial_t N_1 = -\left[1 + \frac{D}{\gamma_{\parallel}}\Delta q^2 - i\frac{\Delta\omega}{\gamma_{\parallel}}\right]N_1 - \sum_j (A_j^* B_{j+1} + A_j B_{j-1}^*), \tag{34}$$

while the evolution of the modal amplitudes is simply given by

$$\partial_t A_j = \kappa(fB_j - A_j), \tag{35}$$

with $f=\Gamma/\kappa$. Since typical values of the diffusion coefficient are $D\sim 50\ \mathrm{cm}^2/\mathrm{s}$, and the cavity length is of the order of 0.3 mm, the effect of the diffusion term in the equation for N_1 is negligible, so we drop it.

It is worth remarking that the same terms in Eqs. (33)–(35) appear for a multimode unidirectional ring laser. In such a case the details of the derivation change but the final equations are formally equivalent, since, in both configurations, modal coupling arises from slow spatiotemporal variation of carrier density. Thus, in principle, we can expect the same type of multimode dynamics in either Fabry-Pérot or unidirectional ring lasers.

A very last step is to eliminate the coefficient χ_0' in front of χ; this can be done by defining the new variables and the new parameter $\tilde{f}$ as

$$\chi \to \chi_0'\tilde{\chi}, \tag{36}$$

$$A_j \to \frac{\widetilde{A_j}}{\sqrt{\chi_0'}}, \tag{37}$$

$$f \to \frac{\tilde{f}}{\chi_0'}, \tag{38}$$

which yields

$$\tilde{f} = \chi_0 \frac{\Gamma\omega_p v_g}{2cn\kappa}. \tag{39}$$

At this point, a specification for the optical susceptibility has to be given in order to close the problem. We consider the analytical approximation to the susceptibility of a semiconductor medium with quantum-well (QW) structure developed in [11], which reads

$$\chi(\Omega,N) = i\chi_0\left[\ln\left(1 - \frac{b}{u+i}\right) - 2\ln\left(1 - \frac{N/N_t}{u+i}\right)\right], \tag{40}$$

$$u = \frac{\Omega - \Omega_0}{\gamma_\perp}, \tag{41}$$

where χ_0 determines the material gain, $\hbar\Omega_0$ is the energy of the lowest optical transition, N_t is the transparency carrier density, and $\gamma_\perp$ is the inverse of the polarization dephasing time.

The model is thus given by Eqs. (33)–(35), together with Eqs. (30) and (40). The numerical simulations were performed using the parameters $\Delta\omega/(2\pi)=102$ GHz, κ $=100$ GHz, $\tilde{f}=7$, $\gamma_{\parallel}=1$ GHz, and $\gamma_{\parallel}/\gamma_\perp=10^{-4}$. We consider 20 modes distributed under the gain curve, although only a few of them are active, and we label them in order of increasing modal frequency, i.e., the higher the index the bluer the mode. The sequence of dynamical behaviors encountered as the injection current is increased is summarized in Fig. 5. At threshold, which corresponds to $N_{eq}=1.14$, the device starts to emit in a single mode (the one labeled as no. 12), but when the current level reaches $N_{eq}=2.635$, then secondary modes start lasing. Slightly above this current value, the total intensity shows the typical mode beating at very high frequency but the modal intensities are constant in time; hence pure multimode emission occurs. However, upon further increasing the current to $N_{eq}=2.71$ a bifurcation occurs such that the intensity of every active mode starts to oscillate in antiphase at low frequency, leaving the total output power constant. Depending on parameter values, this oscillation may start with small amplitude and reach 100% modulation depth through a sequence of secondary bifurcations as the current is increased, or directly develop this large amplitude cycle. In both cases, however, the total intensity remains essentially constant (the relative oscillation being smaller than 0.1%), and the optical frequency follows a well defined sequence progressing from the blue to the red side of the spectrum. We choose current parameter values such that the oscillations already start with 100% modulation depth, as seen in the experiment (see Fig. 6). Further increase of the current provokes more modes to become active and participate in the dynamics, and the oscillation period continuously decreases as the injection current is increased (see Fig. 7), but no noticeable qualitative changes are observed until the periodicity becomes spoiled.

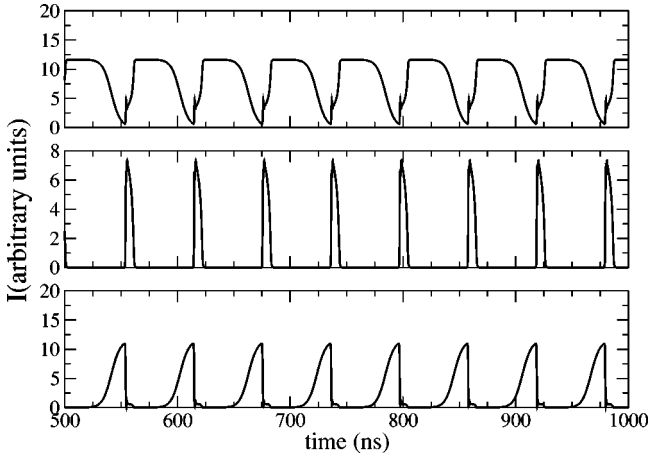

FIG. 6. Numerical results for the intensities of modes no. 11 (top), no. 12 (middle), and no. 13 (bottom) for a current injection $N_{eq}=2.8$.

The origin and characteristics of such oscillations appear closely related to both the four-wave-mixing or population-grating term and the properties of the susceptibility response of semiconductor media.

On one hand, we have checked that by enforcing $N_1\equiv 0$ and thus suppressing the population-grating or four-wave-mixing term, the antiphase square-wave-like oscillations of modal powers disappear, although multimode operation is

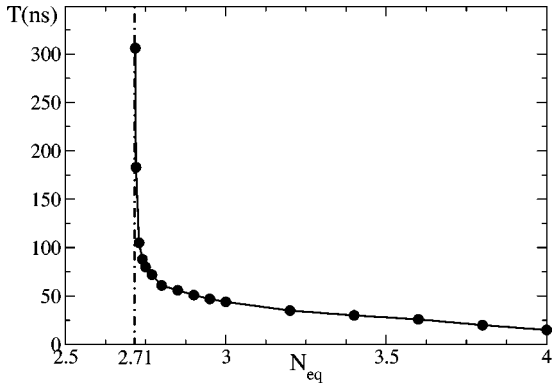

FIG. 7. Period of the oscillation as a function of the injection current.

still possible. Therefore, as found previously in the phenomenological approach, the population-grating contribution (which, in the present approach, cannot be separated from the four-wave-mixing effect) is crucial for the dynamics. In order to control the accuracy of our model we have verified that the inclusion of the higher order terms arising from the second beat note does not modify the observed dynamics, but only changes the bifurcation points slightly. We have also checked that the adiabatic elimination of N_1 leads also to the same kind of dynamics, again with a small displacement of the bifurcation points, confirming that the inclusion of population-grating or four-wave-mixing term is essential for the development of the antiphase oscillations of the modal powers.

On the other hand, the dynamical properties of such an oscillatory regime are characteristic of an asymmetric gain spectrum as provided by the optical susceptibility of QW lasers. We have verified that a two-level-model susceptibility does not lead to the observed dynamics, although it allows for multimode operation. When we artificially break the spectral symmetry of the optical response of a two-level system, the square-wave switching occurs again. Moreover, we have also seen that the sense of the modal sequence is imposed by the relative sign of the derivatives of the real and imaginary parts of the susceptibility respect to the carrier density: in real semiconductor media, the index decreases when the gain increases, thus leading to a progression from blue to red; by artificially reversing the sign of the index change, the sense of the progression is reversed. Thus, the asymmetry of the optical response in semiconductor media imposes a well-defined sense for the progression of the modal dynamics.

VI. SUMMARY AND CONCLUSIONS

The most intriguing and relevant result presented in this article is the observation of a purely deterministic multimode instability with characteristics not reported before. We have demonstrated experimentally that for different free-running multi-longitudinal-mode semiconductor lasers, the modal outputs display large amplitude antiphase oscillations that leave constant the total intensity emitted by the laser. Modal oscillations are in the megahertz range; thus the frequency is much smaller than all frequencies associated with the semiconductor material or the laser cavity round trip. The oscillations are essentially periodic at low pump current values. Such periodicity is progressively destroyed at relatively strong currents.

Our theoretical explanation for the observed dynamics is a four-wave-mixing or population-grating phenomenon, resulting from the interaction among longitudinal modes. The theoretical results are in good agreement with the experimental observations. The appearance of dynamical modal switching requires enhanced four-wave-mixing influence, which directly depends on the differential gain. For smaller differential gain the effect can disappear. This allows us to tackle the question of why these highly organized modal dynamics were not previously observed. It must be noted that classical studies of modal dynamics in semiconductor lasers were performed a long time ago, before the development of QW active regions. These systems provide a larger differential gain than their bulk counterparts, thus leading to enhanced four-wave-mixing effects due to the larger values of $\hat{\chi}$ in Eq. (30). Indeed, our numerical results indicate that for smaller differential gain, the current value for the onset of such oscillations rapidly increases and might even disappear, although the detailed analysis of the bifurcation scenario and its parametric dependencies are currently under investigation.

Furthermore we have shown that a simple phenomenological model, which includes the population-grating and four-wave-mixing term, may also account for the experimental observations. Further work will be necessary to understand the characteristics and properties of the bifurcation sequence leading to this motion and its evolution to a more complicated dynamics.

Note added. Recently, a numerical analysis of a multimode semiconductor laser model has shown some common features with our observations [27].

ACKNOWLEDGMENTS

The work in Bruxelles was supported by the Fonds National de la Recherche Scientifique and the Interuniversity Attraction Pole program of the Belgian government. A. Y. was supported by a grant from FOMEC (Argentina). S. B. acknowledges financial support from MECD (Spain) through sabbatical Grant No. PR2002-0329.

[1] M. Ohtsu and Y. Teramachi, IEEE J. Quantum Electron. **25**, 31 (1989).
[2] S. Inoue, H. Ohzu, S. Machida, and Y. Yamamoto, Phys. Rev. A **46**, 2757 (1992).
[3] R. Linke *et al.*, J. Lightwave Technol. **3**, 706 (1985).
[4] C. Becher, E. Gehrig, and K.-J. Boller, Phys. Rev. A **57**, 3952 (1998).
[5] F. Marin *et al.*, Phys. Rev. Lett. **75**, 4606 (1995).
[6] M. Ohtsu, Y. Teramachi, Y. Otsuka, and A. Osaki, IEEE J. Quantum Electron. **22**, 535 (1986).
[7] G. Agrawal, Phys. Rev. A **37**, 2488 (1988).
[8] M. Homar, S. Balle, and M. San Miguel, Opt. Commun. **131**, 380 (1996).
[9] M. Homar, J. V. Moloney, and M. San Miguel, IEEE J. Quantum Electron. **32**, 553 (1996).
[10] C. Masoller, IEEE J. Quantum Electron. **33**, 796 (1997).
[11] S. Balle, Phys. Rev. A **57**, 1304 (1998).
[12] L. M. Narducci and N. B. Abraham, *Laser Physics and Laser Instabilities* (World Scientific, Singapore, 1988).
[13] A. G. Vladimirov, E. A. Viktorov, and P. Mandel, Phys. Rev. E **60**, 1616 (1999).
[14] L. A. Lugiato, L. N. Narducci, L. V. Eschenazi, D. K. Bandy, and N. B. Abraham, Phys. Rev. A **32**, 1563 (1985).
[15] G. J. de Valcarcel, E. Roldan, and F. Prati, Opt. Commun. **216**, 203 (2003).
[16] E. A. Viktorov and P. Mandel, Phys. Rev. Lett. **85**, 3157 (2000).
[17] T. Baer, J. Opt. Soc. Am. B **3**, 1175 (1986).
[18] R. Roy, C. Bracikowski, and G. E. James, in *Proceedings of the International Conference on Quantum Optics*, edited by R. Inguva and G. S Agarwal (Plenum, New York, 1993), p. 231.
[19] J.-Y. Wang and P. Mandel, Phys. Rev. A **48**, 671 (1993).
[20] G. Huyet, J. K. White, A. J. Kent, S. P. Hegarty, J. V. Moloney, and J. G. McInerney, Phys. Rev. A **60**, 1534 (1999).
[21] G. Agrawal, IEEE J. Quantum Electron. **23**, 860 (1987).
[22] G. Agrawal, J. Opt. Soc. Am. B **5**, 147 (1988).
[23] W. W. Chow, S. K. Koch, and M. Sargent III, *Semiconductor Laser Physics* (Springer-Verlag, Heidelberg, 1994).
[24] M. Yamada and Y. Suematsu, J. Appl. Phys. **52**, 2653 (1981).
[25] A. P. Bogatov, P. G. Eliseev, and B. N. Sverlov, IEEE J. Quantum Electron. **11**, 510 (1975).
[26] C. Etrich, P. Mandel, N. B. Abraham, and H. Zeghlache, IEEE J. Quantum Electron. **28**, 811 (1992).
[27] M. Ahmed and M. Yamada, IEEE J. Quantum Electron. **38**, 682 (2002).